New $^{40}Ar/^{39}Ar$ ages reveal contemporaneous mafic and silicic eruptions during the past 160,000 years at Mammoth Mountain and Long Valley caldera, California

Gail A. Mahood[†], Joshua H. Ring[§], Simone Manganelli, and Michael O. McWilliams[#]
Department of Geological and Environmental Sciences, Building 320, 450 Serra Mall, Stanford University, Stanford, California 94305-2115, USA

ABSTRACT

We undertook a $^{40}Ar/^{39}Ar$ study of young mafic and silicic lavas at Mammoth Mountain and the Long Valley caldera (east-central California) to better understand the frequency of these eruptions and the magmatic plumbing system that drives them. Our results show that most of Mammoth Mountain, a lava-dome complex straddling the southwestern topographic rim of the caldera, consists of trachydacite lavas erupted at ca. 68 ka. These ages and new 29- and 41-ka ages for trachydacite lavas in the northwest quadrant of the caldera indicate that these silicic lavas are considerably younger than previously thought. Mafic lavas vented widely in the western third of the caldera in the past 190,000 years, suggesting that this area has not been underlain by large bodies of silicic magma during this interval, as such magma would have prevented the rise of the denser basaltic magma.

We identify four eruptive sequences over the past 190,000 years: the western moat sequence (~190–160 ka), the Mammoth sequence (~120–58 ka), the northwest caldera sequence (~41–29 ka), and the Inyo chain sequence (~9 ka–present). In each eruptive sequence mafic and silicic lavas erupted contemporaneously from spatially associated vents. This suggests that intrusion of alkali basalt into the shallow crust led to the silicic eruptions. If the seismic unrest and deformation of the past three decades is a result of basalt injected beneath Mammoth Mountain and perhaps the western third of the caldera, then there is the possibility of spatially associated small-volume silicic eruptions, which would typically be considerably more explosive. In the past 40,000 years, eruptions have occurred along a N-S linear trend less than 10 km wide, limiting the zone subject to volcanic hazards.

Our data bear on Pleistocene glaciation in the region. Ages of 162 ± 2 ka and 99 ± 1 ka for bracketing mafic lava flows better constrain the age of the Casa Diablo till. Our results provide equivocal support for a suggested anticorrelation between volcanism and glaciation for the past 800,000 years in eastern California (Glazner et al., 1999).

INTRODUCTION

Long Valley caldera in east-central California (Fig. 1) is one of three large intracontinental silicic magmatic systems in the western United States that have produced major ignimbrite eruptions in the past million years. It joined the ranks of the world's "restless calderas" in 1980 when a strong earthquake swarm that included earthquakes as large as M6 occurred along the southern margin of the caldera, and uplift was detected on the adjacent caldera floor. Uplift of the resurgent dome in the center of the caldera and recurring earthquake swarms in the southern moat of the caldera during the subsequent three decades have kept Long Valley caldera a focus of U.S. Geological Survey monitoring activity (Hill et al., 1985; Bailey and Hill, 1990; Langbein et al., 1993; Hill et al., 2002). Concerns about volcanic hazards were heightened by an earthquake swarm in 1989 under Mammoth Mountain (Hill et al., 1990), a 700-m-high lava dome complex that straddles the southwestern topographic rim of the caldera (Fig. 1). Mammoth Mountain is a popular ski resort and is adjacent to the growing population of Mammoth Lakes, a regional center for four-season recreation. Soon after the 1989 swarm, it was discovered that CO_2-saturated soils were responsible for areas of tree kill around Mammoth Mountain (Farrar et al., 1995). The CO_2 emissions and He isotopic ratios in excess of $5R_a$ measured in a fumarole on Mammoth Mountain point to outgassing of mantle-derived basalt (Sorey et al., 1998). Earthquake swarms in 1989, 1992–1993, and 1997–1998 have been attributed to intrusion of a basaltic dike (or dikes) or CO_2-rich hydrous fluids exsolved from them, rising to within 1–3 km of the surface (Langbein et al., 1995; Hill and Prejean, 2005).

In order to better understand the frequency of eruptions and the magmatic plumbing of recent volcanism at Long Valley caldera and Mammoth Mountain, and their implications for assessing volcanic hazards, we undertook a $^{40}Ar/^{39}Ar$ study of the youngest volcanic units there. Our new data improve the quality and quantity of data bearing on the timing of volcanism, for example, showing that the bulk of Mammoth Mountain and the trachydacite lavas in the northwest quadrant of the caldera are considerably younger than previously thought. A significant result of this study is recognition that silicic and mafic volcanism was essentially synchronous for the past 160,000 years. Additionally, the new data enable us to speculate on a proposed anticorrelation between glaciation and volcanism, and on the nature of future volcanic activity likely to be associated with Mammoth Mountain and Long Valley caldera.

Geologic Setting

Long Valley caldera lies on the western margin of the extensional Basin and Range Province, and astride major frontal faults of

[†]E-mail: mahood@stanford.edu
[§]Current address: Department of Science, Nichols School, 1250 Amherst Street, Buffalo, New York 14216, USA.
[#]Current address: Australian Commonwealth Scientific and Industrial Research Organization (CSIRO) Exploration and Mining, Australian Resources Research Center, 26 Dick Perry Avenue, Kensington, WA 6151, Australia; e-mail: Mike.Mcwilliams@csiro.au

GSA Bulletin; March/April 2010; v. 122; no. 3/4; p. 396–407; doi: 10.1130/B26396.1; 5 figures; 1 table; Data Repository item 2009241.

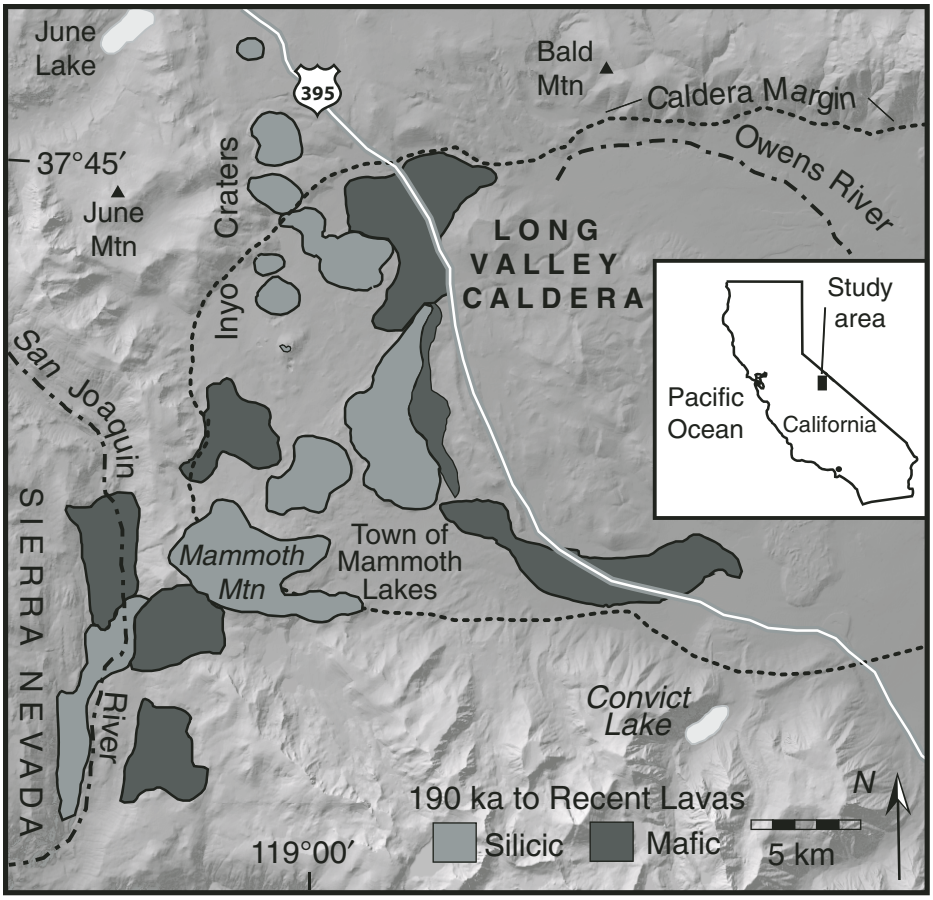

Figure 1. Location map. Study area includes post–190-ka mafic and silicic lavas associated with Mammoth Mountain and the western third of the Long Valley caldera.

the Sierra Nevada that remain active today (Bailey, 1989; Prejean et al., 2002). The caldera formed 0.76 Ma ago due to explosive eruption of 750 km^3 of rhyolitic magma as the Bishop Tuff (Gilbert, 1938; Hildreth and Wilson, 2007), which covered the surrounding landscape with thick ignimbrites and spread ash as far east as the Great Plains (Izett et al., 1970; Bailey et al., 1976). Rhyolite lavas erupted soon after caldera formation in the center of the caldera, and were subsequently uplifted during resurgent doming. Later, rhyolitic lavas erupted in the moat between the resurgent dome and caldera topographic rim at 0.5 and 0.3 Ma (Mankinen et al., 1986; Bailey, 1989).

In the past 190,000 years, eruptions have been largely effusive and have been confined to the western moat of the caldera and the adjacent area between the caldera topographic rim and the canyon of the San Joaquin River (Fig. 2). The most prominent topographic feature is 3370-m Mammoth Mountain, a complex of overlapping alkali rhyolite and trachydacite lava domes and flows (Bailey, 1989), flanked on all sides by lavas of trachydacite, trachyandesite, and trachybasalt. The youngest volcanism in the study area occurred 600 ± 50 a ago in association with intrusion of a composite rhyolite dike along a north-south trend (Miller, 1985; Mastin and Pollard, 1988) that crosses the western moat of the caldera. Magma vented along the northern half of the dike, giving rise to plinian fallout, small pyroclastic flows, and several lava domes. Farther south, magma did not vent, but the trace of the dike is marked by phreatic explosion craters, including the eponymous Inyo Craters, and by ground deformation at Earthquake Fault (Fig. 2).

DESCRIPTION OF UNITS

For consistency, the unit names we apply to the samples we studied are largely those used by Bailey (1989, 2004). The silicic lavas are mineralogically and compositionally diverse, but they can be divided into two suites based on the presence or absence of potassic sanidine ($Or_{60–70}$) as a phenocryst (Ring, 2000). Silicic lavas that erupted in and around Mammoth Mountain do not contain potassic sanidine; if an alkali feldspar is present, it is sodic sanidine ($Or_{40–50}$) or anorthoclase. These lavas range in composition from alkali-feldspar–free trachydacites (Dom, Ddb, Ded, and Def in Fig. 2 and Table 1) to low-silica alkali rhyolites containing sodic sanidine (Rmm and Rlp), along with trachydacites that probably represent mixtures between the two making up most of Mammoth Mountain (Dmm) as well as some of the surrounding flows (Ddp). Silicic units that erupted well north and northeast of Mammoth Mountain contain potassic sanidine as a phenocryst (and/or xenocryst or antecryst). This group includes the northwest caldera trachydacites (Dnw), the low-silicic rhyolites of the Scenic Loop flow (Rsl), Deer Mountain dome (Rdm), and the Inyo lava domes (Ri), and the high-silica rhyolite domes of Mammoth Knolls (Rmk) and Dry Creek (Rdc) (Fig. 2). The mafic lavas consist of trachybasalts to trachyandesites containing 1%–15% phenocrysts of plagioclase, clinopyroxene, and olivine in varying proportions.

The locations of dated samples are shown in Figure 2. The geology shown is simplified; hence, nearly all the patches of mafic units consist of multiple lava flows that can be distinguished and mapped individually based on phenocryst abundance and assemblage. The same is true for several of the silicic units, which consist of separate flows and domes. As a result, patches that are the same color on the map can have samples with different ages.

^{40}Ar/^{39}Ar RESULTS

The ^{40}Ar/^{39}Ar analyses were performed on phenocrysts of sanidine, sodic sanidine, plagioclase, or biotite separated from silicic lavas and one rhyolitic fall deposit (sample M-3) and from microcrystalline devitrified groundmass separated from the mafic lavas and one phenocryst-poor trachydacite. ^{40}Ar/^{39}Ar ages obtained from step-heating experiments are presented in Table 1, and typical age spectra are illustrated in Figure 3. The complete data for the analyses, along with a description of the separation techniques and argon analytical procedures, are available in GSA Data Repository Table DR1.[1] We summarize the results and discuss the quality of the analyses below.

[1]GSA Data Repository item 2009241, Mineral separation and argon analytical techniques and data tables for ^{40}Ar/^{39}Ar analyses, is available at http://www.geosociety.org/pubs/ft2009.htm or by request to editing@geosociety.org.

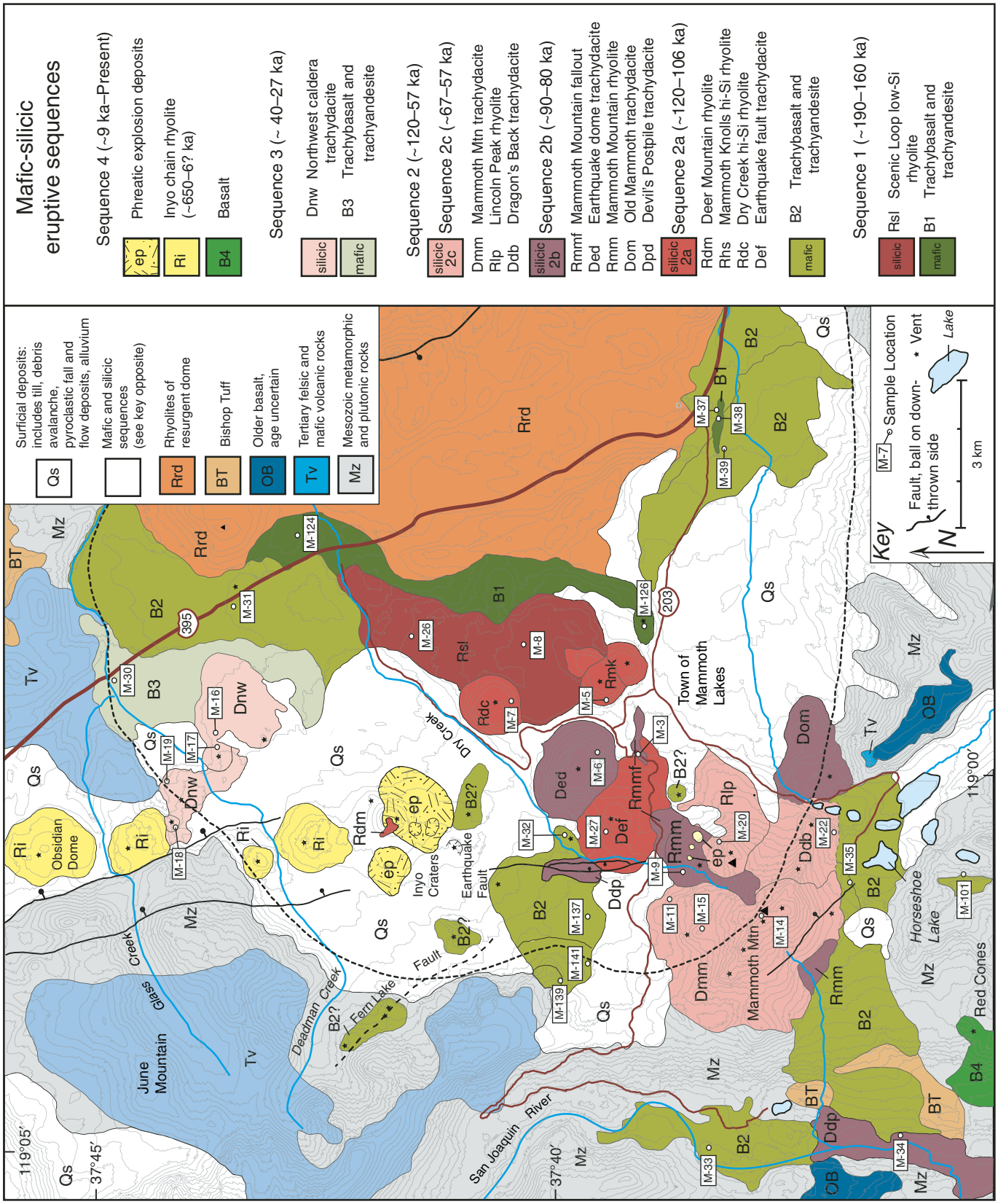
Mafic-silicic eruptive sequences
Sequence 4 (~9 ka–Present)
ep Phreatic explosion deposits
Ri Inyo chain rhyolite (~650–6? ka)
B4 Basalt
Sequence 3 (~ 40–27 ka)
silicic Dnw Northwest caldera trachydacite
mafic B3 Trachybasalt and trachyandesite
Sequence 2 (~120–57 ka)
silicic 2c Sequence 2c (~67–57 ka)
Dmm Mammoth Mtn trachydacite
Rlp Lincoln Peak rhyolite
Ddb Dragon's Back trachydacite
silicic 2b Sequence 2b (~90–80 ka)
Rmmf Mammoth Mountain fallout
Ded Earthquake dome trachydacite
Rmm Mammoth Mountain rhyolite
Dom Old Mammoth trachydacite
Dpd Devil's Postpile trachydacite
silicic 2a Sequence 2a (~120–106 ka)
Rdm Deer Mountain rhyolite
Rhs Mammoth Knolls hi-Si rhyolite
Rdc Dry Creek hi-Si rhyolite
Def Earthquake fault trachydacite
mafic B2 Trachybasalt and trachyandesite
Sequence 1 (~190–160 ka)
silicic Rsl Scenic Loop low-Si rhyolite
mafic B1 Trachybasalt and trachyandesite
Surficial deposits: includes till, debris avalanche, pyroclastic fall and flow deposits, alluvium
Qs
Mafic and silicic sequences (see key opposite)
Rhyolites of resurgent dome
Rrd
Bishop Tuff
BT
Older basalt, age uncertain
OB
Tertiary felsic and mafic volcanic rocks
Tv
Mesozoic metamorphic and plutonic rocks
Mz
Key
Sample Location
Vent
Fault, ball on down-thrown side
Lake
N
3 km
119°05′
37°45′
37°40′
119°00′
June Mountain
Glass Creek
Obsidian Dome
Deadman Creek
Fern Lake
Fault
Inyo Craters
Earthquake Fault
Dry Creek
Town of Mammoth Lakes
Mammoth Mtn
Horseshoe Lake
Red Cones
San Joaquin River
203
395

Figure 2.

Figure 2. Sample locations and geologic map of the western moat of Long Valley caldera, Mammoth Mountain, and adjacent areas. Geology based on Bailey (1989). Not immediately apparent from the map, the western moat (the area between the western caldera margin and the resurgent dome) is filled with mafic lavas (Vogel et al., 1994), many of which vented from the area beneath what is now Mammoth Mountain (W. Hildreth, 2007, personal commun.) and are now mantled by till and/or pyroclastic debris from the 600-a-old Inyo Craters eruption. Patches of basalt on the map consist of multiple lava flows that can be distinguished on phenocryst content and chemical composition. One mafic lava sample, M-148, is located south of the map at Pumice Buttes, ~4 km from Red Cones.

TABLE 1. NEW $^{40}Ar/^{39}Ar$ AGES FOR SILICIC AND MAFIC LAVAS FROM MAMMOTH MOUNTAIN AND THE WESTERN MOAT OF LONG VALLEY CALDERA, CALIFORNIA

				Age spectrum				Isochron analysis		
Map unit	Sample number	Material dated	Total fusion age ±1σ (ka)	Number of steps, increments used (°C)	^{39}Ar (%)	$^{40}Ar_{rad}$ (%)	Plateau WMA ±1σ (ka)	$^{40}Ar/^{36}Ar$ intercept ±1σ	Isochron age ±1σ (ka)	MSWD
Silicic units										
Sequence #3										
Dnw	M-16§	Sanidine	24 ± 1	4, 1000–1075	51	16	27 ± 1	297 ± 3	26 ± 3	0.3
Dnw	M-17†	Sanidine	32 ± 1	11, 850–1250	92	16	30 ± 1	295 ± 2	31 ± 2	0.6
Dnw	M-17†	Biotite	44 ± 3	5, 1025–1200	67	0.6	42 ± 3	295.9 ± 0.2	33 ± 8	0.4
Dnw	M-18§	Sanidine	38 ± 1	5, 775–1050	81	18	40 ± 1	298 ± 4	38 ± 2	0.01
Dnw	M-19†	Sanidine	37 ± 1	4, 1075–1350	93	32	41 ± 1	278 ± 13	45 ± 5	2.9
Sequence #2c										
Ddb	M-22§	Plag	111 ± 2	5, 850–1100	73	4.0	58 ± 2	295 ± 1	59 ± 5	1.0
Rlp	M-20†	Na-san	63 ± 2	6, 950–1150	68	5.6	65 ± 2	294 ± 1	71 ± 7	0.2
Rlp	M-20†	Biotite	47 ± 3	6, 975–1200	78	0.9	No plateau	2902 ± 2	150 ± 45	39
Dmm	M-11†	Na-san	79 ± 1	6, 850–1150	84	23	67 ± 1	297 ± 4	67 ± 3	1.9
Dmm	M-14§	Na-san	82 ± 1	6, 900–1250	83	33	68 ± 1	293 ± 9	69 ± 4	14
Dmm	M-15†	Na-san	65 ± 1	7, 950–1275	99	12	68 ± 1	290 ± 2	74 ± 4	3.8
Dmm	M-14§	Biotite	91 ± 2	4, 850–1000	86	12	96 ± 2	299 ± 5	88 ± 12	4.7
Dmm	M-15†	Biotite	126 ± 5	8, 850–1175	83	2.8	119 ± 4	294 ± 1	140 ± 12	1.0
Sequence #2b										
Rmm	M-9§	Na-san	123 ± 3	3, 900–100	56	41	81 ± 1	314 ± 15	74 ± 6	0.01
Ded	M-6†	Plag	143 ± 2	3, 1050–1200	69	11	87 ± 2	297 ± 2	85 ± 4	1.2
Rmmf	M-3#1§	Na-san	107 ± 6	4, 650–900	73	21	88 ± 6	270 ± 12	115 ± 19	0.5
Rmmf	M-3#2§	Na-san	91 ± 2	5, 800–1100	64	45	91 ± 2	301 ± 6	90 ± 2	0.1
Ddp	M-34†	Grndms	95 ± 1	4, 850–1050	84	23	98 ± 1	298 ± 5	95 ± 6	0.4
Sequence #2a										
Def	M-27§	Plag	284 ± 7	4, 900–1100	66	15	113 ± 2	296 ± 5	111 ± 9	2.1
Rmk	M-5†	San	110 ± 1	7, 950–1400	97	56	113 ± 1	292 ± 3	111 ± 2	2.1
Rmk	M-5†	Biotite	171 ± 6	7, 850–1075	96	4.6	No plateau	295 ± 4	136 ± 25	52
Rmk	M-7†	Biotite	110 ± 2	6, 1075–1250	89	5.9	143 ± 2	296 ± 1	140 ± 5	4.5
Sequence #1										
Rsl	M-8§	San	164 ± 2	3, 850–1050	65	81	163 ± 2	296 ± 8	162 ± 2	0.9
Rsl	M-26†	San	165 ± 2	9, 850–1175	81	65	161 ± 2	287 ± 4	163 ± 2	1.1
Rsl	M-26§	Biotite	210 ± 3	4, 950–1100	90	11	No plateau	290 ± 2	227 ± 15	16
Mafic lavas										
Sequence #3										
M3	M-30†	Grndms	29 ± 2	4, 850–950	64	3.1	31 ± 2	298 ± 3	21 ± 11	0.04
Sequence #2c										
M2	M-31†	Grndms	6 ± 5	4, 850–1000	85	1.8	66 ± 2	295 ± 4	68 ± 8	2.3
Sequence #2b										
M2	M-35†	Grndms	82 ± 1	6, 850–1400	96	6.1	81 ± 1	296 ± 2	82 ± 22	3.5
M2	M-33†	Grndms	76 ± 1	4, 800–950	89	15	82 ± 1	309 ± 11	61 ± 16	1.1
M2	M-141#	Grndms	95 ± 67	6, 700–950	92	2.1	87 ± 7	294 ± 1	99 ± 4	0.9
M2	M-137#	Grndms	89 ± 60	6, 600–1000	98	5.8	88 ± 5	290 ± 3	97 ± 6	2.5
M2	M-168#	Grndms	84 ± 70	6, 600–1000	93	2.5	91 ± 7	293 ± 2	100 ± 9	3.1
M2	M-139#	Grndms	95 ± 49	7, 600–950	96	2.0	94 ± 9	296 ± 1	93 ± 10	32
M2	M-39†	Grndms	89 ± 2	4, 800–950	68	11	99 ± 1	293 ± 3	108 ± 16	0.02
M2	M-37†	Grndms	95 ± 2	4, 800–950	82	3.4	100 ± 2	294 ± 1	113 ± 14	2.6
Sequence #2a										
M2	M-101#	Grndms	98 ± 101	4, 600–900	89	1.6	105 ± 7	288 ± 2	140 ± 8	1.5
M2	M-149#	Grndms	111 ± 81	4, 700–850	74	5.0	118 ± 10	287 ± 2	157 ± 27	33
M2	M-32†	Grndms	67 ± 4	4, 850–1000	83	4.2	121 ± 3	296 ± 2	115 ± 13	5.3
Sequence #1										
M1	M-148#	Grndms	150 ± 44	7, 600–950	93	4.6	142 ± 5	294 ± 2	153 ± 16	4.1
M1	M-126#	Grndms	142 ± 45	5, 700–900	84	1.4	148 ± 14	294 ± 1	165 ± 24	25
M1	M-38†	Grndms	156 ± 2	4, 800–950	60	15	162 ± 2	293 ± 2	169 ± 7	0.05
M1	M-124A#	Grndms	190 ± 71	8, 600–1000	99	4.3	193 ± 7	293 ± 1	215 ± 7	2.0
M1	M-124B#	Grndms	113 ± 60	6, 700–950	55	7.2	190 ± 9	292 ± 3	208 ± 16	3.6

Note: The plateau weighted mean age (WMA) is calculated by weighting increments by the proportion of ^{39}Ar produced. The $\%^{40}Ar_{rad}$ is the aggregated value for the increments used in calculating the WMA. The isochron age and intercept are calculated using the steps that were included in calculating the plateau WMA. For the three biotite samples that do not yield plateaus, the isochrons are calculated using the steps listed under "Age spectrum." In doing data reduction, an age of 28.34 Ma for the Taylor Creek sanidine monitor was used for samples with numbers less than M-100, and an age of 1.19 Ma for the Alder Creek sanidine monitor was used on samples with numbers greater than M-100.

†Irradiated 1 hr in the Oregon State University cadmium-lined reactor with the 28.34-Ma Taylor Creek sanidine monitor.

§Irradiated 30 min in the Oregon State University cadmium-lined reactor with the 28.34-Ma Taylor Creek sanidine monitor.

#Irradiated 30 min in the Oregon State University cadmium-lined reactor with the 1.19-Ma Alder Creek sanidine monitor.

Abbreviations: Grndms—groundmass; plag—plagioclase; san—sanidine; MSWD—mean square of weighted deviations.

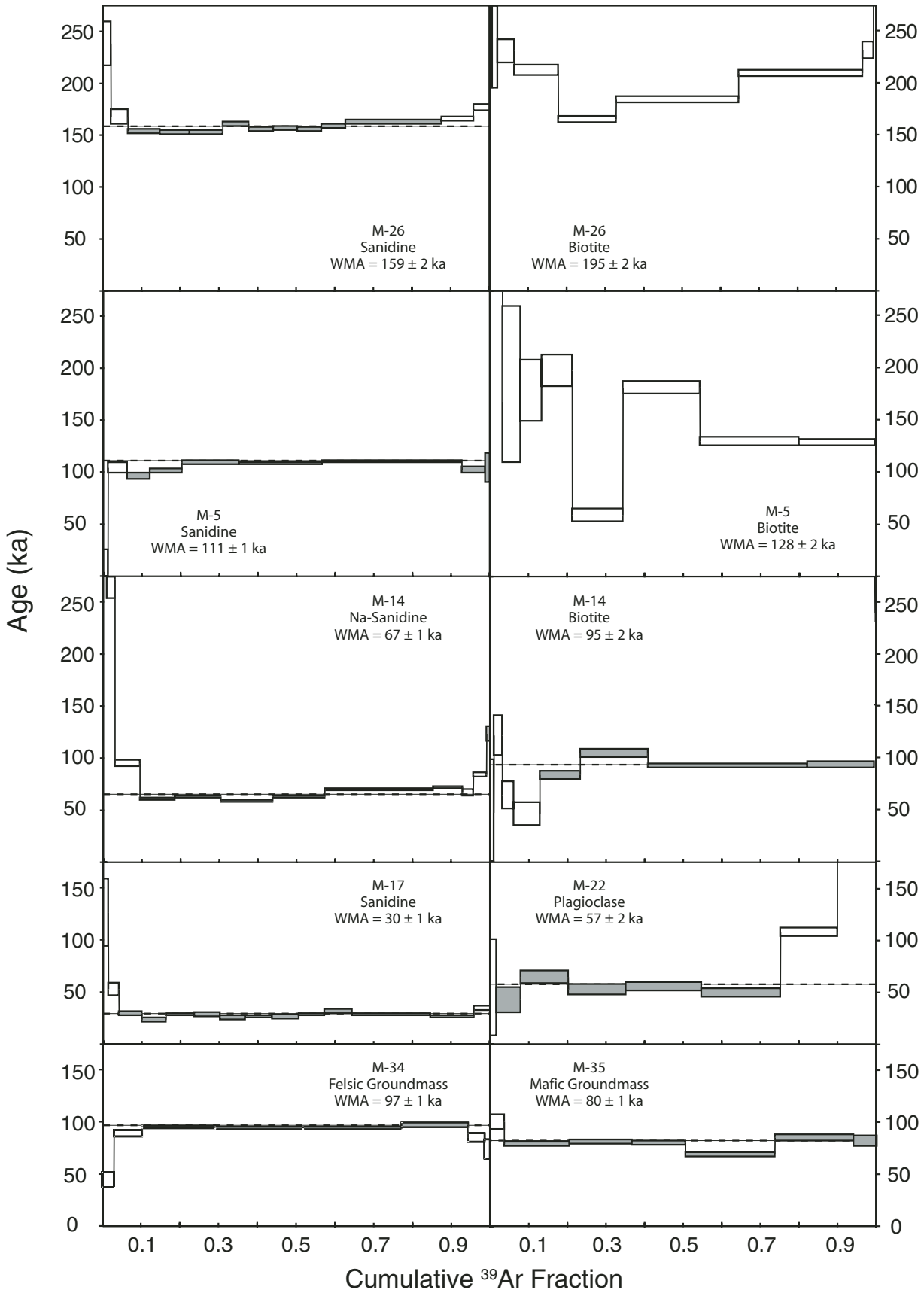
M-26
Sanidine
WMA = 159 ± 2 ka
M-26
Biotite
WMA = 195 ± 2 ka
M-5
Sanidine
WMA = 111 ± 1 ka
M-5
Biotite
WMA = 128 ± 2 ka
M-14
Na-Sanidine
WMA = 67 ± 1 ka
M-14
Biotite
WMA = 95 ± 2 ka
M-17
Sanidine
WMA = 30 ± 1 ka
M-22
Plagioclase
WMA = 57 ± 2 ka
M-34
Felsic Groundmass
WMA = 97 ± 1 ka
M-35
Mafic Groundmass
WMA = 80 ± 1 ka
Age (ka)
Cumulative 39Ar Fraction

Figure 3.

Figure 3. $^{40}Ar/^{39}Ar$ age spectra illustrating the range in quality of data for different materials analyzed. Steps used in calculating plateau weighted mean age (WMA) shaded in gray. Boxes are ±1σ. WMA indicated by dashed line. Sanidine, sodic sanidine, and groundmass produce good to excellent spectra with well-defined plateaus. Plagioclase has high-temperature steps that are anomalously old. Biotites yield older apparent ages than coexisting sanidine or sodic sanidine, no matter whether a spectrum is saddle-shaped, scattered, or has an acceptable plateau. See text for discussion.

Silicic Units

Feldspar

All 14 analyses of sanidine or sodic sanidine yielded steps that agreed within 2σ with the possible exception of the lowest- and/or highest-temperature steps. In most cases the steps that are outliers at the 2σ level agree at the 3σ level. These lowest- and highest-temperature steps typically contain very little gas, and their lack of agreement at 2σ suggests that either we have underestimated the uncertainties of the analyses slightly or the samples contain small amounts of excess argon (but not enough to drive the isochron intercept values measurably from atmospheric). The latter is a possibility given that nearly all the silicic lavas and many of the basalts contain evidence of magma mixing (Ring, 2000).

The majority of the sanidine and sodic sanidine analyses yielded a high-quality result with a well-defined plateau age that agrees with the isochron and total-fusion ages. Eight of the sanidine or sodic sanidine separates analyzed yielded plateaus at 1σ (i.e., there are at least three contiguous steps in the age spectrum that agree within 1σ and account for more than 60% of the ^{39}Ar released) (e.g., M-5 and M-17 in Fig. 3). The remaining six analyses met this criterion at the 2σ level (e.g., M-26 and M-14 in Fig. 3).

In the absence of independent evidence for whether the samples contain a small amount of excess argon or we have underestimated analytical uncertainties, we took a conservative approach in computing the plateau weighted mean ages (WMAs) reported in Table 1. Rather than exclude apparently high-precision steps that do not agree at 1σ but do agree at 2σ, we generally included contiguous steps that agree at 2σ, with the exceptions of lowest- and highest-temperature steps with large uncertainties. We did this even if a sample yielded a plateau using only steps that agree at 1σ. The same approach was taken with data reduction for all analyses in this study.

The three plagioclase separates from trachydacites yielded steps that agree at the 2σ level except for the lowest- and highest-temperature steps. The steps define plateaus at the 2σ level. The total-fusion ages are significantly older than the WMAs, in each case a result of the highest-temperature steps, accounting for 12%–28% of the ^{39}Ar, having apparent ages that are more than twice as old as the plateau ages and are clearly too old based on stratigraphic relationships (e.g., M-22 in Fig. 3).

Groundmass

We analyzed groundmass for one phenocryst-poor trachydacite (M-34 in Fig. 3). The steps agree at the 2σ level except for the lowest- and highest-temperature steps. The data define a plateau at the 1σ level (Fig. 3).

Biotite

Of the seven biotite analyses, three (M-5, M-20, and M-26 in Table 1) yielded steps that do not agree within 2σ, even excluding the highest- and lowest-temperature steps. The age spectra for these analyses do not have plateaus by our criterion, and two have saddle-shaped spectra (e.g., M-26 in Fig. 3).

All of the remaining four samples have steps that agree at 2σ with the exception of the lowest- and highest-temperature steps. Despite yielding satisfactory plateaus at 2σ (e.g., M-14 in Fig. 3), as discussed below, all four WMAs appear to be too old based on comparisons with feldspar ages and stratigraphic relationships.

Mafic Lavas

For the eight groundmass samples from mafic lavas with sample numbers less than M-100, all the steps agreed within 2σ, with the exception of some of the lowest- and highest-temperature steps. All samples yielded plateaus at 2σ (e.g., M-35 in Fig. 3), and a few samples meet this criterion at the 1σ level.

The ten mafic lavas with sample numbers greater than M-100 were analyzed at a different time when system blanks were larger. As a result, individual steps have greater analytical uncertainties, and the agreement between steps is not as good. This is reflected in the significantly larger uncertainties reported for the WMAs for these samples in Table 1.

Precision and Accuracy

We favor the use of plateau WMAs for analyses with well-defined plateaus because isochron ages are typically not as well defined for young volcanic samples with low radiogenic yields (Lanphere, 2000), and because they appear to be more accurate for our feldspar and groundmass analyses. For the samples of sanidine and basalt groundmass for which we did replicate analyses (M-3 and M-124, respectively, in Table 1), the WMAs agree better than the total-fusion and isochron ages. This is also the case for feldspar from lavas that based on field relations we believe to be of similar age (M-16 and M-17; M-18 and M-19; and M-11, M-14, and M-15).

Feldspar separates (sanidine, Na-sanidine, and plagioclase) yielded the best WMA results, with precision ranging from ~1.3% for the 162-ka rhyolite to 3.8% for the 29-ka trachydacites. The WMAs for feldspars are generally in excellent agreement with the isochron ages, presumably because the extraneous Ar correction is small (because the radiogenic Ar yield is relatively high), and its value is close to atmospheric argon. Groundmass WMAs exhibit good precision (typically <4%) and good agreement with isochron ages. The exceptions are some of the basalts with sample numbers greater than M-100, which were analyzed with larger system blanks, resulting in those samples with radiogenic argon yields below 3% having calculated precisions as large as 10%.

An independent measure of the precision of the analyses is provided by replicate analysis of sanidine sample M-3 at 88 ± 6 and 91 ± 2 ka (WMA) and of basalt groundmass sample M-124 at 193 ± 7 and 190 ± 9 ka. (All reported errors on ages are 1σ.) Feldspar separated from two different samples of the Scenic Loop rhyolite lava (M-8 and M-26) yielded WMAs of 163 ± 2 and 161 ± 2 ka; the calculated total-fusion and isochron ages are also slightly more than 160 ka. Feldspar from three samples of trachydacite lavas collected on Mammoth Mountain, which, based on their morphology and colinear vents, we believe erupted all at about the same time, yielded WMAs of 67 ± 1, 68 ± 1, and 68 ± 1 (M-11, M-14, and M-15). Similarly, the two trachydacite domes in the northwest quadrant of the caldera (M-18 and M-19) with relatively subdued topography, due in part to cover by pyroclastic debris, yielded feldspar WMAs of 40 ± 1 and 41 ± 1, whereas the two domes (M-16 and M-17) that overlie them have steeper margins, and are the source of the pyroclastic debris, have ages of 27 ± 1 and 30 ± 1. This agreement of the argon ages with the relative ages determined in the field also bears on the accuracy of the feldspar and

groundmass analyses. Another example is provided by a stack of three mafic lava flows in the south moat, in ascending order M-38, M-37, and M-39, which yielded ages of 162 ± 2, 100 ± 2, and 99 ± 1, respectively.

Mankinen et al. (1986) preferred the feldspar ages over the biotite ages for the silicic lavas because they were more consistent with stratigraphic relations and their paleomagnetic data. New, more detailed mapping by Wes Hildreth (2007, personal commun.) demonstrates that the Mankinen et al. (1986) biotite ages for lavas in and around Mammoth Mountain are too old to be consistent with stratigraphic relationships, and that some of our biotite ages are older than our feldspar or groundmass ages for underlying lavas. We also prefer the feldspar ages because the feldspar data are more precise (due to higher radiogenic argon yield), and because three of the seven biotite analyses did not yield satisfactory plateaus, suggesting that at least some biotite contains detectable excess argon.

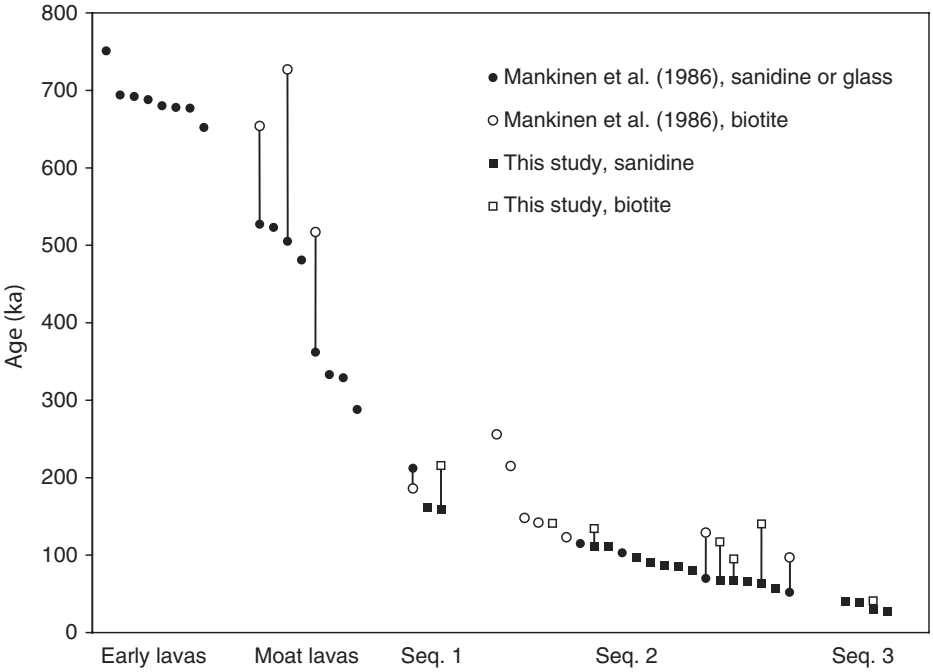

Figure 4. Comparison of biotite ages with those for feldspar, glass, and groundmass for silicic units, illustrating the discordance of the biotite ages. Samples are arranged in order of sanidine or groundmass age. For the Sequence 1 lava in which the Mankinen et al. (1986) biotite age appears to be the younger of the pair, the uncertainty on the biotite date is so large that it overlaps at the 1σ level.

Anomalously Old Ages for Biotite

Biotite separates yield older ages than coexisting feldspars for the six samples for which both were analyzed, sometimes as much as twice as old. These differences are significant at 2σ.[2] Mankinen et al. (1986) observed a similar discordance going back to the moat rhyolites (although due to the lower precision of the K-Ar ages, the differences were significant at 2σ for only one pair). We illustrate the discordance of the biotite ages by plotting our data and those of Mankinen et al. (1986) in Figure 4. The wide range of old biotite ages is exemplified by the data for the trachydacitic domes and flows that compose the bulk of Mammoth Mountain (Dmm). Our three feldspar dates are concordant at 67–68 ka, whereas two biotite separates yield statistically different WMAs of 96 ± 2 ka and 119 ± 4 ka. Mankinen et al. (1986) obtained biotite ages of 97 ± 25 ka and 129 ± 65 ka on samples from the same area.

Our petrographic observations suggest a possible explanation for the older biotite ages. A number of lavas, including trachydacites of Mammoth Mountain, the trachydacites of the northwest caldera, and the 162-ka, low-silica rhyolite, contain resorbed plagioclase containing biotite inclusions. If the rounded cores are xenocrystic or older cognate material and the radiogenic argon within the included biotites was not completely reset, then liberation of these biotite grains during crushing and their incorporation into the biotite separates would produce anomalously older ages. The fact that isochron plots do not show evidence for the incorporation of excess argon may be due to poor control on determining the $^{40}Ar/^{36}Ar$ intercept value. Biotite from samples M-26 (Fig. 3) and M-20 exhibits saddle-shaped spectra typical of the incorporation of excess argon (Lanphere and Dalrymple, 1976).

COMPARISON WITH PREVIOUS WORK

Our sanidine ages are not significantly different from sanidine K-Ar ages obtained on the same silicic units by Bailey et al. (1976) and Mankinen et al. (1986), but the $^{40}Ar/^{39}Ar$ ages are more precise (Fig. 5). The use of K-Ar biotite ages in interpreting the eruptive history of Mammoth Mountain led Bailey et al. (1976) to estimate an age too old for the start of volcanism and to overestimate the time required to construct the edifice. Our results suggest a younger and shorter period of eruptions between ~113 and 58 ka, with the main bulk of the mountain (represented by unit Dmm; Fig. 2) forming in 1000 years or less at 68 ka (based on $^{40}Ar/^{39}Ar$ ages from three separate lava domes on Mammoth Mountain; weighted average: 68 ± 1, Table 1).

The trachydacites in the northwest part of the caldera (Dnw) had not been dated previously and were grouped by Bailey (1989) with the trachydacitic units on and around Mammoth Mountain. Our new eruption ages indicate that these trachydacites are significantly younger than those on Mammoth Mountain, having erupted in two clusters at 41 ± 1 and 29 ± 1 ka (weighted averages in Table 1).

Heumann (1999) determined $^{40}Ar/^{39}Ar$ ages, as reported in Heumann et al. (2002), by incremental heating experiments on bulk sanidine separates for several of the units studied here. They reported indistinguishable isochron ages of 147 ± 4 and 151 ± 4 on two samples of the Scenic Loop low-silica rhyolite (Rsl in Fig. 2), compared to our WMAs of 161 ± 2 and 163 ± 2 ka for two samples of the same lava flow. Mankinen et al. (1986) determined K-Ar ages of 154 ± 72 ka, 155 ± 28 ka, and 149 ± 16 ka for the same lava flow. Heumann et al. (2002) reported an isochron age of 109 ± 3 on the northern Mammoth Knolls lava dome (Rmk in Fig. 2)

[2]We considered whether the lower radiogenic yields of biotites coupled with an inaccurate value for $^{40}Ar/^{39}Ar$ machine mass discrimination could cause the apparent anomalously older ages. This seems unlikely, however, because in sample M-20 (Rlp) both the Na-sanidine and biotite separates had low radiogenic yields; yet the biotite still gave an older age. Furthermore, the fact that the K-Ar work done in the U.S. Geological Survey laboratories also yields older biotite ages suggests that the older ages are not due to an internal laboratory problem.

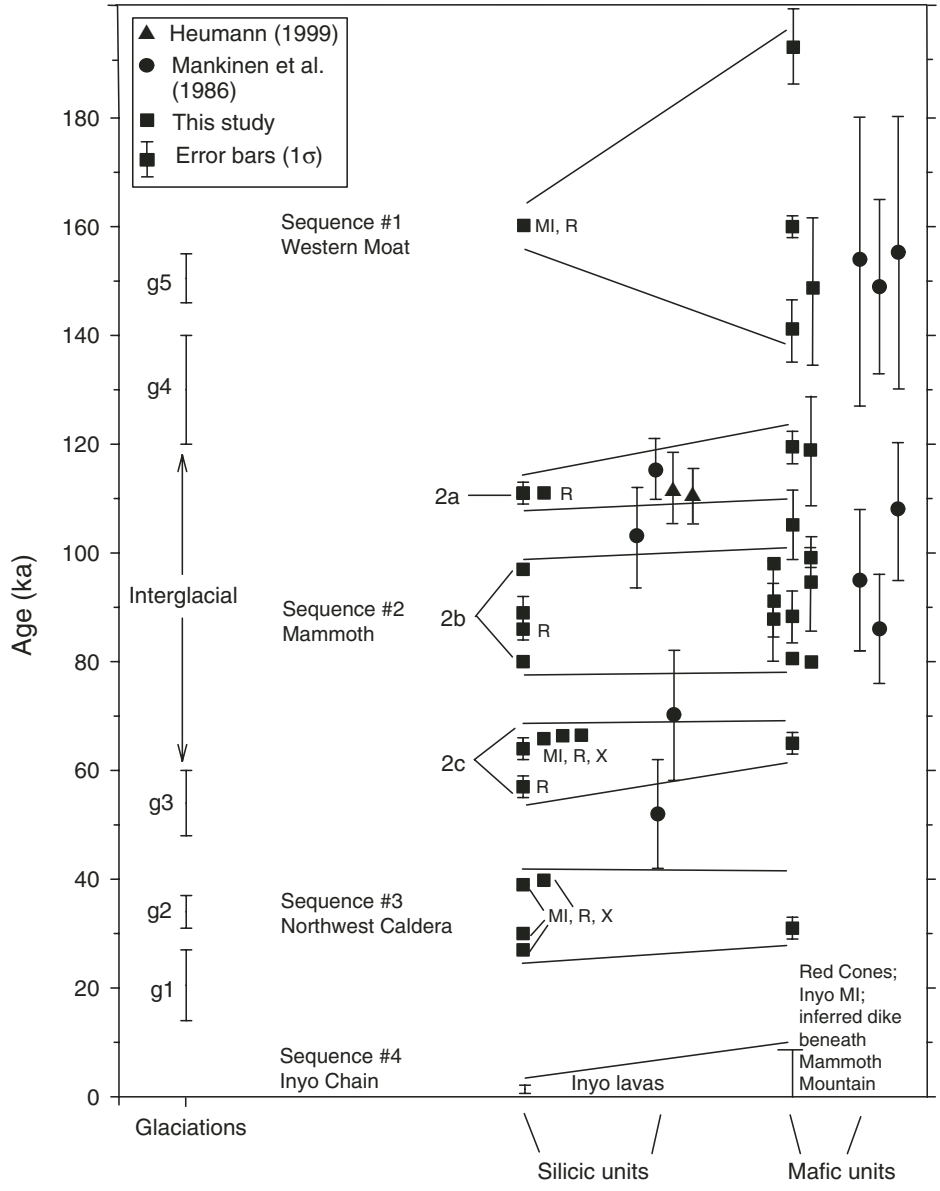

Figure 5. Eruptive sequences for the past 190,000 years in Long Valley caldera, Mammoth Mountain, and adjacent areas. Error bars are 1σ errors. Where no bar is shown, the size of the symbol encompasses the 1σ error bars. Silicic and mafic lavas erupted contemporaneously in four sequences, the most recent one continuing to the present day. The start date of Sequence 4 is poorly constrained but is certainly postglacial (see text for discussion). Most of the silicic lavas show evidence for the interaction of multiple magmas (Ring, 2000), including mafic magmas and magmas that are only slightly more or less mafic than the host, as evidenced by magmatic inclusions (MI), strongly resorbed phenocrysts (R), and xenocrysts/antecrysts (X).

for which we obtained a WMA of 113 ± 1 on sanidine. They dated two other nearby lava flows that, based on similar topographic expression and high-silica rhyolite composition, are likely to have erupted at around the same time: the southern Mammoth Knolls dome (Rmk in Fig. 2) yielding an isochron age of 111 ± 5 ka, and the Dry Creek dome (Rdc) at 112 ± 6 ka. Although more precise, the $^{40}Ar/^{39}Ar$ ages are indistinguishable from the sanidine K-Ar ages of 97 ± 12, 106 ± 8, and 110 ± 22 ka obtained from the same three domes by Mankinen et al. (1986). We did not analyze a sample from the Deer Mountain dome (Rdm in Fig. 2). Heumann et al. (2002) report a plateau age of 101 ± 8, within error of the 115 ± 6 K-Ar age determined earlier by Mankinen et al. (1986).

To augment the number of age determinations for mafic eruptions, we dated lava flows different from those studied by Bailey et al. (1976) and Mankinen et al. (1986). Our ages for mafic units are in agreement with the range of dates reported in the earlier studies. The significant advantage of the greater precision of our $^{40}Ar/^{39}Ar$ ages is that it makes it possible to show that mafic and silicic lavas in and adjacent to the western third of Long Valley caldera repeatedly erupted in tandem during several short episodes over the past 160,000 years. The basaltic and silicic eruptions were therefore spatially and temporally correlated.

MAFIC AND SILICIC VOLCANIC SEQUENCES

Accepting the eruption ages given by $^{40}Ar/^{39}Ar$ feldspar and groundmass ages, we find that, in and adjacent to the western third of Long Valley caldera, mafic and silicic magmas erupted contemporaneously in several episodes over the past 160,000 years (Fig. 5). The correlation is not only temporal, but appears to be roughly spatial (Fig. 2), with vents for both mafic and silicic lavas for each sequence being located near one another. Hence we have defined four eruptive sequences in Figure 5: (1) the western moat sequence (~190–160 ka), (2) the Mammoth sequence (~120–58 ka), (3) the northwest caldera sequence (~41–29 ka), and (4) the Inyo chain sequence (~9 ka–Present).

Sequence 1: Western Moat (~190–160 ka)

The oldest dated lava in the western moat is a porphyritic trachybasalt for which we obtained replicate WMAs of 193 ± 7 and 190 ± 9 (M-124 in Table 1). The oldest silicic eruptive unit exposed in the western moat is the Scenic Loop low-silica rhyolite (Rsl, Fig. 2), which Bailey et al. (1976) included as part of their Moat rhyolite series. It yielded sanidine WMAs of 161 ± 2 and 163 ± 2 ka from samples from two different localities (Table 1), within the uncertainties of the ages obtained by Mankinen et al. (1986) and Heumann et al. (2002) for the same lava flow. A trachyandesite flow (M-38, Fig. 2) southeast of the 162-ka Scenic Loop rhyolite flow yielded an identical WMA of 162 ± 2 ka (Table 1). Therefore, there is strong evidence that mafic and silicic magmas vented contemporaneously in the western moat of the caldera at ca. 160 ka.

Previous K-Ar studies reported ages for mafic units in the western caldera as old as ca. 400 ka (Curry, 1971; Bailey et al., 1976; Mankinen

et al., 1986); such dates, however, are either inconsistent on duplicate runs or have large errors that render them not statistically different from the oldest dated mafic units of our study. $^{40}Ar/^{39}Ar$ step-heating experiments on basalts from the Inyo-4 drill core yielded ages as old as 445 ± 82 ka (Vogel et al., 1994), but these samples may contain excess ^{40}Ar. Further work is needed to determine if mafic lavas erupted in the western caldera moat prior to 190,000 years ago, and whether there are any buried rhyolites that are older than 162 ka.

We obtained an age of 142 ± 5 ka (M-148 in Table 1) for a mafic lava from Pumice Buttes, which is located off Figure 2, ~4 km south of Red Cones. This is the only sample for which we have obtained an age between 190 and 120 ka that vented outside the western caldera moat.

Sequence 2: Mammoth (~120–57 ka)

Following approximately 40,000 years of quiescence in the western caldera, a new eruptive sequence began, the most voluminous of the series. Mafic lavas spread widely throughout the study area, and silicic lavas erupted in and adjacent to the southwestern quadrant of the caldera (Fig. 2). There are enough high-quality data from our study and that of Mankinen et al. (1986) and Heumann et al. (2002) to subdivide the silicic units of Sequence 2 into three episodes (Fig. 5 and Table 1): (2A) eruptions of trachydacite and low- and high-silica rhyolite lavas in the southwestern moat of the caldera at Deer Mountain, Dry Creek Dome, Mammoth Knolls, and Earthquake Fault at ca. 113 ka (Rdm, Rdc, Rmk, and Def in Fig. 2); (2B) eruptions of trachydacite and low-silica rhyolite lavas inside and just outside the southwestern caldera topographic margin at ~98–81 ka (Ded, Dom, Ddp, and Rmm); and (2C) eruptions of trachydacite and rhyolite domes and flows that make up the bulk of Mammoth Mountain and Lincoln Peak at ~68–58 ka (Dmm, Ddb, and Rlp).

Mafic lavas vented widely in the moat and outside the caldera to the south and west of Mammoth Mountain (Fig. 2). In a general way, the mafic lavas can also be subdivided into the same three episodes as the silicic lavas, but the larger analytical errors for the ages of mafic lavas make these assignments less certain. Recent mapping and chemical correlations by Wes Hildreth indicate that many of the lavas vented from beneath what is now Mammoth Mountain (2007, personal commun.). A trachybasaltic cinder cone north of Mammoth Mountain (M-32 in Fig. 2) is the oldest dated unit of this sequence, with a WMA of 121 ± 3 ka (Table 1). The youngest date determined for a mafic unit of this eruptive sequence was for a trachyandesitic flow (WMA: 66 ± 2 ka, M-31 in Fig. 2; Table 1). Other mafic units around the base of Mammoth Mountain erupted between ~105 and 81 ka (Fig. 2), including the lava flow that flowed down the canyon of the San Joaquin River, ponding to form the columnar basalt that is the main attraction in the Devils Postpile National Monument.

Sequence 3: Northwest Caldera (~29–40 ka)

After approximately 20,000 years of quiescence, trachydacite and trachybasalt erupted along a northwest trend from the northwestern moat across the topographic rim of the caldera (Fig. 2). Two small trachydacite domes erupted along the caldera margin at 41 ± 1 ka (weighted average, Table 1). Overlying one of them are two younger trachydacite domes that erupted at 29 ± 1 ka. An adjacent trachybasaltic lava is similar in age (31 ± 2 ka; Table 1) to the younger trachydacite domes. These lavas had not been dated previously. Bailey (1989) assigned them to the same group as the trachydacites of Mammoth Mountain.

These trachydacitic lavas, erupted at 41 and 29 ka, represent a young, previously unrecognized, period of volcanism in the northwestern quadrant of the caldera. Our new younger ages for the northwest caldera lavas suggest a greater temporal continuity between volcanism in the moat and volcanism to the north of the caldera in the Inyo Chain and at Mono Craters.

Sequence 4: Inyo Chain (~9 ka–Present)

The most recent eruptions (Sequence 4) in and adjacent to the western third of Long Valley caldera took place along the north-trending Inyo volcanic chain (Wood, 1984; Miller, 1985). Vents for lavas of Sequences 2 and 3 tend to be oriented in northwest-southeast chains (e.g., the top of Mammoth Mountain, along the Fern Lake fault, the high-silica rhyolite domes of Dry Creek and Mammoth Knolls, and the northwest caldera trachydacite domes in Fig. 2), whereas the vents for Sequence 4 are aligned more or less north-south, as are the active faults with dip-slip motion in the region. This change in vent alignment suggests a shift in extension direction in the past 30,000 years.

The oldest Inyo chain unit is a small, high-silica rhyolite lava dome just north of Deadman Creek (Fig. 2). Its age is poorly constrained. It is overlain by a Mono Craters fallout layer that yielded an age of 1190 ± 80 ^{14}C yr B.P. (Wood, 1984). Based on hydration rind measurements, Wood suggested an age of 10–27 ka. Miller (1985) reinterpreted Wood's data as indicating an age of ca. 6 ka. We have assigned it to Sequence 4 (rather than Sequence 3) because of its chemical similarities to the 600-a-old Inyo Craters lava domes.

Wilson Butte is a rhyolitic lava dome that erupted just north of the map area of Figure 2. Its age is estimated at ca. 1350 a based on charcoal samples from associated pyroclastic flows (Miller, 1985).

About 600 ± 50 years ago, a composite rhyolitic dike intruded along a north-south trend (Miller, 1985; Mastin and Pollard, 1988) that intersects the western edge of the Long Valley caldera. Magma vented along the northern half of the trend, giving rise to plinian fallout, small pyroclastic flows, and lava domes that exhibit magma mingling of coarsely porphyritic and finely porphyritic rhyolite (Sampson and Cameron, 1987; Bailey, 1989; Vogel et al., 1989). Along the southern part, magma did not vent, but the presence of the dike is indicated by the phreatic explosion deposits (ep in Fig. 2) and craters at Deer Mountain and the Inyo Craters, and, even farther south, by ground deformation at Earthquake Fault (Fig. 2). Phreatic explosion deposits on the northern flank of Mammoth Mountain (Fig. 2), which yield charcoal with a ^{14}C age of 500 ± 200 yr B.P. (Bailey, 1989) but are overlain by the 600-a-old Inyo fallout, lie on a southward continuation of the trend.

No mafic lavas within the caldera or along the Inyo chain trend have been identified as contemporaneous with Sequence 4. Cinder cones and lava flows at Red Cones (B4 in Fig. 2) are unglaciated and therefore Holocene (Bailey, 1989). Charcoal bracketing an ash layer correlated to Red Cones gives an age of ca. 9 ka (Bursik, 2004). Evidence for involvement of mafic magma in the 600-a-old Inyo Craters eruptions is the sparse mafic magmatic inclusions present in the rhyolitic lavas (Varga et al., 1990).

Recurring earthquake swarms in the south moat and deformation of the floor of Long Valley caldera since 1980 have been attributed by some workers to intrusion of magma beneath the resurgent dome and in the south moat (see references summarized in Hill et al., 1985; also Langbein et al., 1995; Battaglia et al., 1999), although there is some debate about how much of the seismicity and deformation are due to regional tectonic activity and changes in the hydrothermal system, rather than magma intrusion (Prejean et al., 2002).

There is strong evidence that mafic magma has been intruded recently beneath Mammoth Mountain. Earthquake swarms beneath the mountain in 1989, 1992–1993, and 1997–1998 and ground deformation along a leveling line following Route 203 (Fig. 2) have been attributed to intrusion of a basaltic dike (or dikes) or CO_2-rich hydrous fluids exsolved from them

rising to within a few km of the surface (Hill et al., 1990; Langbein et al., 1995; Prejean et al., 2003; Hill and Prejean, 2005). Emission of CO_2 gas, which has killed trees in several areas ringing Mammoth Mountain, most prominently north of Horseshoe Lake (Fig. 2), and helium isotope ratios >5 Ra measured in a fumarole on Mammoth Mountain are consistent with outgassing of mantle-derived basalt emplaced beneath Mammoth Mountain (Farrar et al., 1995; Sorey et al., 1998). It would appear that eruptive Sequence 4 is still ongoing.

DISCUSSION

Volcanism and Glacial Intervals

There has been some debate on the age of the Casa Diablo Till, which lies between mafic lavas on the southwestern floor of the Long Valley caldera (Curry, 1971; Bailey et al., 1976; Mankinen et al., 1986). Based on K-Ar ages of the sandwiching basaltic flows, Curry (1971) assigned an age of ca. 400 ka to the till. Later work indicated an age younger than 126 ka, but K-Ar ages obtained from different aliquots of the same sample yielded discordant results (Bailey et al., 1976; Mankinen et al., 1986). We dated groundmass separates from a trachyandesitic flow that underlies the till (M-38) and a trachybasaltic flow that overlies the till (M-39). Our bracketing ages of 162 ± 2 ka and 99 ± 1 ka are consistent with the results of Bailey et al. (1976) and Mankinen et al. (1986). This age range encompasses both late Stage 6 and early Wisconsin time, but the lack of evidence in the sediment record of Owens Lake, some 50 km south of Long Valley caldera, for a prominent Stage 5e suggests that the last interglacial lasted from 120 to 60 ka in the eastern Sierra Nevada (Bischoff et al., 1997). If so, the Casa Diablo till was deposited during the Tahoe (Stage 6) glaciation.

Based on a compilation of existing ages for volcanic rocks over a large area of eastern California, Glazner et al. (1999) suggested an anticorrelation between volcanism and glaciation for the past 800,000 years. Accordingly, we compare in Figure 5 our eruptive ages with the five major glacial intervals proposed by Bischoff et al. (1997) for the eastern Sierra: (1) g1, 14–27 ka; (2) g2, 31–37 ka; (3) g3, 48–60 ka; (4) g4, 120–140 ka; and (5) g5, 146–155 ka. Lavas corresponding in age to glacial periods g4 and g5 are absent or scarce. Two mafic lavas (M-126 and M-148 in Table 1) have WMAs of 148 ± 14 ka and 142 ± 5 ka, respectively, but given their precisions, it is not possible to say whether they erupted during glacial or nonglacial intervals. Soon after the end of glacial interval g4, volcanism began in the southwestern quadrant of the caldera and continued through the long interglacial period from 120 to 60 ka. Our third eruptive sequence encompasses glaciation g2 (31–37 ka) of Bischoff et al. (1997); however, given the precisions of the ages, it is also possible that the eruptions occurred just before glaciation g2 and in the short interglacial period between g2 and g1. A better understanding of the magnitude and timing of Sierran glaciations (e.g., the g2 glacial period does not seem to be represented in the total inorganic carbon record in the Owens Lake core [Benson et al., 1996]) as well as a more detailed dating study of more units over a broader period of time are required to test the hypothesis of Glazner et al. (1999). It also remains to be determined how glacial loading or unloading—both having been implicated in triggering eruptions (Sigvaldason et al., 1992)—could directly impact volcanism on the caldera floor or at the even lower elevations of Owens Valley.

Implications of the New Ages for the State of the Long Valley Magmatic System

Evidence for sizable bodies of silicic magma, let alone a large integrated magma chamber, beneath the Long Valley caldera at the present time is weak. There has been no volcanism in the eastern two-thirds of the caldera in the past 300,000 years. Heat flow is low in the eastern half of the caldera, and the largest positive heat flow anomaly is near Mammoth Mountain (Lachenbruch et al., 1976). Modeling of the caldera geothermal system indicates that the zone of hot-water upflow lies beneath the western part of the caldera and that fluids cool progressively as they flow eastward (Sorey et al., 1991). It appears that the eastern two-thirds of the caldera is no longer a focus of magmatic activity.

In the past 160,000 years, all eruptive activity has occurred in the western moat of the caldera and in and around Mammoth Mountain (Hildreth, 2004). During this interval, trachybasalts and trachyandesites vented widely, suggesting that the area has not been underlain by an extensive body (or bodies) of silicic magma. Were such a body of silicic magma beneath the western third of the caldera, it would have created a "shadow zone" for basaltic eruptions by preventing these denser mafic magmas from reaching the surface. Any residue remaining from the magma chamber that was rejuvenated during eruption of the early rhyolites and resurgent doming following caldera collapse must now be sufficiently crystalline (i.e., >65%) to sustain brittle fracture and allow passage of mafic dikes.

Any silicic magma bodies during the past 160,000 years must have been small and/or short-lived. The absence of a large integrated reservoir is consistent with the diversity of whole-rock chemical and isotopic compositions and phenocryst assemblages of the silicic lavas, with the lack of systematic temporal trends in compositions of the magmas erupted, and the evidence for many of the silicic lavas being complex mixtures of magmas and xenocrystic material (Fig. 2; Heumann and Davies, 1997; Ring, 2000). This petrographic and geochemical heterogeneity contrasts with magmas erupted from the upper parts of large magma chambers, which are buffered, physically and thermally, from intrusion of magma below and, therefore, tend to be more homogeneous.

The Role of Mafic Magma in Generating Silicic Magmas and Triggering Silicic Eruptions

The fact that mafic lavas have erupted contemporaneously with trachydacites and rhyolites, commonly from vents in close proximity, suggests that introduction of basalt into the shallow crust has induced some or most of the silicic eruptions. Injection of basalt can trigger eruptions from existing magma bodies by overpressuring the magma chamber to the point that dikes propagate upward from it or by causing exsolution of a volatile phase in the silicic magma by heating it (e.g., Sparks et al., 1977; Bachmann and Bergantz, 2003). If basalt were injected into a largely crystallized silicic magma body, the silicic magma might be remobilized by reduction in viscosity due to loss of crystals. The heat released by cooling and crystallizing the basalt could also melt near-solidus granite (e.g., Huppert and Sparks, 1988). If that granite were similar in composition to the rhyolitic Bishop Tuff and moat lavas, the near-eutectoid composition and the low heats of fusion of most of the minerals would facilitate melting and the production of low-crystallinity magmas (Mahood, 1990). Introduction of basaltic or andesitic magma into the shallow crust might alternatively lead to silicic eruptions by creating new silicic magma through fractional crystallization. Such silicic magma might erupt shortly after being generated or it could be triggered into eruption by a later intrusion of mafic or intermediate magma.

CONCLUSIONS

The results of our $^{40}Ar/^{39}Ar$ study of the youngest volcanic units associated in and around the Long Valley caldera have implications for volcanic hazards. We show that the main edifice of Mammoth Mountain was constructed by eruption of trachydacite lavas over a short period of about a thousand years

(or perhaps less) at ca. 68 ka. This age and the 41- and 29-ka ages for the trachydacite lavas in the northwest quadrant of the caldera make these units considerably younger than previously thought, and they demonstrate continuity of silicic magmatism in the western moat of the Long Valley caldera, perhaps overlapping with the earliest eruptions at Mono Craters.

We interpret the eruptive record as indicating that the Long Valley system proper has been in decline since the eruptions in the south moat 300,000 years ago, and that the current magmatic activity in the study area is focused in a narrow north-south zone associated with extensional faulting along the Sierran range front. In the past 40,000 years, volcanism has been limited to a north-south belt stretching ~50 km, from south of Mammoth Mountain through the study area to the north shore of Mono Lake (Bailey, 1989; Hildreth, 2004). In the area of the Long Valley caldera, this belt is less than 10 km wide.

During each of the four temporally and spatially distinct eruptive sequences over the past 160,000 years, mafic and silicic lavas erupted contemporaneously. Mafic lavas vented widely throughout the western third of the caldera, suggesting that the western moat was not underlain during the past 190,000 years by an extensive body or bodies of silicic magma, which would have prevented the eruption of the denser basaltic magma. The proximity of contemporaneous vents for silicic and mafic lavas and the petrologic evidence for lavas being complex magma mixtures suggest that silicic eruptions were in many cases triggered by intrusion of alkali basalt and trachyandesite into the shallow crust.

Our finding that mafic and silicic eruptions have been contemporaneous in the past 160,000 years has implications for volcanic hazards assessment in the context of intrusions of magma inferred beneath the south moat and resurgent dome of Long Valley caldera since the early 1980s and the inferred intrusion of basalt beneath Mammoth Mountain in 1989 (Hill et al., 2002). This means that if basalt is being injected, spatially associated silicic eruptions are a possibility, with the risk of far more explosive eruptions than typical basaltic outbursts. The venting of mafic magmas in the western third of the Long Valley caldera suggests that any residual Long Valley magma body below is in such an advanced state of crystallization that it cannot readily be triggered into a voluminous ignimbrite-forming eruption by intrusion of a few tenths of a cubic kilometer of basalt. Hence, the likely silicic products are lava flows or domes, perhaps with associated small-volume plinian fallout and pyroclastic flows. Any eruptions at Mammoth Mountain would carry with them the hazards associated with eruption on a steep snow-covered mountain—surges, block-and-ash flows, and lahars (Ring, 2000). The recognition that future volcanism is likely to be restricted to the narrow north-south strip of the Mammoth-Inyo-Mono trend, and be dominated by effusive activity (and perhaps associated phreatomagmatic outbursts) aids in the construction of hazard maps.

ACKNOWLEDGMENTS

We dedicate this paper to Charles Gilbert (1910–1988) and Roy Bailey (1929–2003), who laid the groundwork for all the subsequent studies of the Long Valley caldera and Mammoth Mountain. We thank A. Calvert, T. Dumitru, M. Grove, L. Heister, and J. Hourigan for assistance with the argon analyses and data reduction, and M. Coble for assistance with figure preparation. W. Hildreth, G. Maddy, N. Flint, and L. Pic collaborated on sample collection. We thank reviewers M. Reid and P. Renne and Associate Editor N. Riggs for constructive reviews that improved the manuscript. Ring's M.S. thesis research was supported by a Penrose Student Grant 529-99 from the Geological Society of America and by a McGee Fund grant from the Stanford School of Earth Sciences.

REFERENCES CITED

Bachmann, O., and Bergantz, G.W., 2003, Rejuvenation of the Fish Canyon magma body: A window into the evolution of large-volume silicic magma systems: Geology, v. 31, p. 789–792, doi: 10.1130/G19764.1.

Bailey, R.A., 1989, Geologic map of the Long Valley caldera, Mono-Inyo Craters volcanic chain, and vicinity, eastern California: U.S. Geological Survey Miscellaneous Field Studies Map MF-1933, scale 1:62,500, 2 sheets.

Bailey, R.A., 2004, Eruptive history and chemical evolution of the precaldera and postcaldera basalt-dacite sequences, Long Valley, California: Implications for magma sources, current seismic unrest, and future volcanism: U.S. Geological Survey Professional Paper 1692, 75 p.

Bailey, R.A., and Hill, D.P., 1990, Magmatic unrest at Long Valley Caldera, California, 1980–1990: Geoscience Canada, v. 17, p. 175–179.

Bailey, R.A., Dalrymple, G.B., and Lanphere, M.A., 1976, Volcanism, structure, and geochronology of Long Valley Caldera, Mono County, California: Journal of Geophysical Research, v. 81, p. 725–743, doi: 10.1029/JB081i005p00725.

Battaglia, M., Roberts, C., and Segall, P., 1999, Magma intrusion beneath Long valley caldera confirmed by temporal changes in gravity: Science, v. 285, p. 2119–2122, doi: 10.1126/science.285.5436.2119.

Benson, L.V., Burdett, J.W., Kashgarian, M., Lund, S.P., Phillips, F.M., and Rye, R.O., 1996, Climatic and hydrologic oscillations in the Owens Lake basin and adjacent Sierra Nevada, California: Science, v. 274, p. 746–748, doi: 10.1126/science.274.5288.746.

Bischoff, J.L., Menking, K.M., Fitts, J.P., and Fitzpatrick, J.A., 1997, Climatic oscillations 10,000–155,000 B.P. at Owens Lake, California, reflected in glacial rock flour abundance and lake salinity in Core OL-92: Quaternary Research, v. 48, p. 313–325, doi: 10.1006/qres.1997.1933.

Bursik, M., 2004, http://www.volcano.buffalo.edu:9090/mmvz/index_html.

Curry, R.R., 1971, Glacial and Pleistocene history of the Mammoth Lakes Sierra, California: A geologic guidebook: University of Montana Geological Series Publication no. 11, p. 1–49.

Farrar, C.D., Sorey, M.L., Evans, W.C., Howle, J.F., Kerr, B.D., and Kennedy, B.M., 1995, Forest-killing diffuse CO_2 emission at Mammoth Mountain as a sign of magmatic unrest: Nature, v. 376, p. 675–678, doi: 10.1038/376675a0.

Gilbert, C.M., 1938, Welded tuff in eastern California: Geological Society of America Bulletin, v. 49, p. 1829–1862.

Glazner, A.F., Manley, C.R., Marron, J.S., and Rojstaczer, S., 1999, Fire or ice: Anticorrelation of volcanism and glaciation in California over the past 800,000 years: Geophysical Research Letters, v. 26, p. 1759–1762, doi: 10.1029/1999GL900333.

Heumann, A., 1999, Longevity of silicic magma chambers [Ph.D. thesis]: Amsterdam, Netherlands, Vrije Universiteit Amsterdam.

Heumann, A., and Davides, G.R., 1997, Isotopic and chemical evolution of the post-caldera rhyolitic system at Long Valley, California: Journal of Petrology, v. 38, p. 1661–1678.

Heumann, A., Davies, G.R., and Elliott, T., 2002, Crystallization history of rhyolites at Long Valley, California, inferred from combined U-series and Rb-Sr isotope systematics: Geochimica et Cosmochimica Acta, v. 66, p. 1821–1837, doi: 10.1016/S0016-7037(01)00883-3.

Hildreth, W., 2004, Volcanological perspectives on Long Valley, Mammoth Mountain, and Mono Craters: Several contiguous but discrete systems: Journal of Volcanology and Geothermal Research, v. 136, p. 169–198, doi: 10.1016/j.jvolgeores.2004.05.019.

Hildreth, W., and Wilson, C.J.N., 1997, Compositional zoning of the Bishop Tuff: Journal of Petrology, v. 48, p. 951–999, doi: 10.1093/petrology/egm007.

Hill, D.P., and Prejean, S., 2005, Volcanic unrest beneath Mammoth Mountain, California: Journal of Volcanology and Geothermal Research, v. 146, p. 257–283, doi: 10.1016/j.jvolgeores.2005.03.002.

Hill, D.P., Bailey, R.A., and Ryall, A.S., 1985, Active tectonic and magmatic processes beneath Long Valley Caldera, eastern California: An overview: Journal of Geophysical Research, v. 90, p. 11,111–11,120, doi: 10.1029/JB090iB13p11111.

Hill, D.P., Ellsworth, W.L., Johnston, M.J.S., Langbein, J.O., Oppenheimer, D.H., Pitt, A.M., Reasenberg, P.A., Sorey, M.L., and McNutt, S.R., 1990, The 1989 earthquake swarm beneath Mammoth Mountain, California: An initial look at the 4 May through 30 September activity: Bulletin of the Seismological Society of America, v. 80, p. 325–339.

Hill, D.P., Dzurisin, D., Ellsworth, W.L., Endo, E.T., Galloway, D.L., Gerlach, T.M., Johnston, M.J.S., Langbein, J., McGee, K.A., Miller, C.D., Oppenheimer. C., and Sorey, M.L., 2002, Response plan for volcano hazards in the Long Valley caldera and Mono Craters region, California: U.S. Geological Survey Bulletin 2185, 57 p.

Huppert, H., and Sparks, S.J., 1988, The generation of granitic magmas by intrusion of basalt into continental crust: Journal of Petrology, v. 29, p. 599–624.

Izett, G.A., Wilcox, R.F., Powers, H.A., and Desborough, G.A., 1970, The Bishop ash bed, a Pleistocene marker bed in the western United States: Quaternary Research, v. 1, p. 121–132, doi: 10.1016/0033-5894(70)90014-1.

Lachenbruch, A.H., Sass, J.H., Munroe, R.J., and Moses, T.H., 1976, Geothermal setting and simple heat conduction models for the Long Valley caldera: Journal of Geophysical Research, v. 81, p. 769–784, doi: 10.1029/JB081i005p00769.

Langbein, J., Hill, D.P., Parker, T.N., and Wilkinson, S.K., 1993, An episode of reinflation of the Long Valley caldera, eastern California: 1989–1991: Journal of Geophysical Research, v. 98, p. 15,851–15,870, doi: 10.1029/93JB00558.

Langbein, J., Dzurisin, D., Marshall, G., Stein, R., and Rundle, J., 1995, Shallow and peripheral volcanic sources of inflation revealed by modeling two-color geodimeter and leveling data from Long Valley caldera, California: Journal of Geophysical Research, v. 100, p. 12,487–12,495, doi: 10.1029/95JB01052.

Lanphere, M.A., 2000, Comparison of conventional K-Ar and $^{40}Ar/^{39}Ar$ dating of young mafic volcanic rocks: Quaternary Research, v. 53, p. 294–301, doi: 10.1006/qres.1999.2122.

Lanphere, M.A., and Dalrymple, G.B., 1976, Identification of excess ^{40}Ar by the $^{40}Ar/^{39}Ar$ age spectrum technique: Earth and Planetary Science Letters, v. 32, p. 141–148, doi: 10.1016/0012-821X(76)90052-2.

Mahood, G.A., 1990, Second reply to comment of R.S.J. Sparks, H.E. Huppert, and C.J.N. Wilson on: "Evidence for long residence times of rhyolitic magma in the Long Valley magmatic system: The isotopic record in the precaldera lavas of Glass Mountain": Earth and Planetary Science Letters, v. 99, p. 395–399, doi: 10.1016/0012-821X(90)90145-N.

Mankinen, E.A., Gromme, C.S., Dalrymple, G.B., Lanphere, M.A., and Bailey, R.A., 1986, Paleomagnetism and K-Ar ages of volcanic rocks from the Long Valley Caldera, California: Journal of Geophysical Research, v. 91, p. 633–652, doi: 10.1029/JB091iB01p00633.

Mastin, L.G., and Pollard, D.P., 1988, Surface deformation and shallow dike intrusion processes at Inyo Craters, Long Valley, California: Journal of Geophysical Research, v. 93, p. 13,221–13,235, doi: 10.1029/JB093iB11p13221.

Miller, C.D., 1985, Holocene eruptions at the Inyo volcanic chain, California: Implications for possible eruptions in Long Valley Caldera: Geology, v. 13, p. 14–17, doi: 10.1130/0091-7613(1985)13<14:HEATIV>2.0.CO;2.

Prejean, S., Ellsworth, W., Zoback, M., and Waldhauser, F., 2002, Fault structure and kinematics of the Long Valley Caldera region, California, revealed by high-accuracy earthquake hypocenters and focal mechanism stress inversions: Journal of Geophysical Research, v. 107, doi: 10.1029/2001JB001168.

Prejean, S., Stork, A., Ellsworth, W., Hill, D., and Julian, B., 2003, High precision earthquake locations reveal seismogeneic structure beneath Mammoth Mountain, California: Geophysical Research Letters, v. 30, doi: 10.1029/2003GL018334.

Ring, J.H., 2000, Young volcanism in western Long Valley caldera, California [M.S. thesis]: Stanford University, 136 p.

Sampson, D.E., and Cameron, K.L., 1987, The geochemistry of the Inyo volcanic chain: Multiple magma systems in the Long Valley region, eastern California: Journal of Geophysical Research, v. 92, p. 10,403–10,421, doi: 10.1029/JB092iB10p10403.

Sigvaldason, G.E., Annertz, K., and Nilsson, M., 1992, Effect of glacier loading/deloading on volcanism: Postglacial volcanic production rate of the Dyngjufjoll area, central Iceland: Bulletin of Volcanology, v. 54, p. 385–392, doi: 10.1007/BF00312320.

Sorey, M.L., Suemnicht, G.A., Sturchio, N.C., and Nordquist, G.A., 1991, New evidence on the hydrothermal system in Long Valley Caldera, California, from wells, fluid sampling, electrical geophysics, and age determinations of hot spring deposits: Journal of Volcanology and Geothermal Research, v. 48, p. 229–263.

Sorey, M.L., Evans, W.C., Kennedy, B., Farrar, C.D., Hainsworth, L.J., and Hausback, B., 1998, Carbon dioxide and helium emissions from a reservoir of magmatic gas beneath Mammoth Mountain, California: Journal of Geophysical Research, v. 103, p. 15,303–15,323, doi: 10.1029/98JB01389.

Sparks, S.R.J., Sigurdsson, H., and Wilson, L., 1977, Magma mixing: Mechanism for triggering acid explosive eruptions: Nature, v. 267, p. 315–318, doi: 10.1038/267315a0.

Varga, R.J., Bailey, R.A., and Suemnicht, G.A., 1990, Evidence for 600-year-old basalt and magma mixing at Inyo Craters volcanic chain, Long Valley caldera, California: Journal of Geophysical Research, v. 95, p. 21,441–21,450, doi: 10.1029/JB095iB13p21441.

Vogel, T.A., Eichelberger, J.C., Younker, L.W., Schuraytz, B.C., Horkowitz, J.P., Stockman, H.W., and Westrich, H.R., 1989, Petrology and emplacement dynamics of intrusive and extrusive rhyolites of Obsidian Dome, Inyo Craters Volcanic Chain, eastern California: Journal of Geophysical Research, v. 94, p. 17,937–17,956.

Vogel, T.A., Woodburne, T.B., Eichelberger, J.C., and Layer, P.W., 1994, Chemical evolution and periodic eruption of mafic lava flows in the west moat of Long Valley Caldera, California: Journal of Geophysical Research, v. 99, p. 19,829–19,842, doi: 10.1029/94JB00897.

Wood, S., 1984, Chronology of Late Pleistocene and Holocene volcanics, Long Valley and Mono Basin geothermal areas, eastern California: U.S. Geological Survey Open-File Report 83-747, 76 p.

Manuscript Received 26 December 2007
Revised Manuscript Received 10 October 2008
Manuscript Accepted 13 October 2008

Printed in the USA